INSTITUTE OF PHYSICS PUBLISHING JOURNAL OF OPTICS B: QUANTUM AND SEMICLASSICAL OPTICS

J. Opt. B: Quantum Semiclass. Opt. **4** (2002) S52–S57 PII: S1464-4266(02)30546-9

Holographic generation and orbital angular momentum of high-order Mathieu beams

S Chávez-Cerda[1,4], M J Padgett[2], I Allison[2], G H C New[1], J C Gutiérrez-Vega[3], A T O'Neil[2], I MacVicar[2] and J Courtial[2]

[1] Quantum Optics and Laser Science Group, Imperial College, London SW7 2BW, UK
[2] Department of Physics and Astronomy, University of Glasgow, Glasgow G12 8QQ, UK
[3] Instituto Nacional de Astrofisica, Optica y Electrónica, Apartado Postal 51/216, Puebla, Mexico 72000

E-mail: j.courtial@physics.gla.ac.uk

Received 6 November 2001, in final form 4 February 2002
Published 8 March 2002
Online at stacks.iop.org/JOptB/4/S52

Abstract
We report the first experimental generation of high-order Mathieu beams and confirm their propagation invariance over a limited range. In our experiment we use a computer-generated phase hologram. The peculiar behaviour of the vortices in Mathieu beams gives rise to questions about their orbital-angular-momentum content, which we calculate by performing a decomposition in terms of Bessel beams.

Keywords: Computer-generated holograms, orbital angular momentum of light, diffraction-free beams

1. Introduction

Ever since Durnin's description of Bessel beams [1, 2], diffraction-free light beams, of which Bessel beams were the first non-trivial example, have been the subject of intense theoretical and experimental interest. Potential applications of non-diffracting optical and ultrasonic beams range from lithography [3] through optical communications [4] to medical imaging [5].

The history of diffraction-free beams started with Durnin's realization that in Whittaker's solution [6, 7] to the Helmholtz equation,

$$u(x, y, z > 0) = \exp(\mathrm{i}k_z z) \int_0^{2\pi} A(\phi) \times \exp(\mathrm{i}k_r (x \cos\phi + y \sin\phi))\, \mathrm{d}\phi \quad (1)$$

the intensity $|u(x, y, z)|^2$ is independent of z, and the beams it represents are therefore diffraction-free [1]. Durnin investigated the case $A(\phi) = \text{const.}$, and found that the resulting field u is given by

$$u(r, z > 0) \propto \exp(\mathrm{i}k_z z) J_0(k_r r) \quad (2)$$

where J_0 is a Bessel function (of the first kind). Such a beam is known as a zero-order Bessel beam. It was later found that functions $A(\phi) \propto \exp(\mathrm{i}m\phi)$ lead to higher-order Bessel beams [8], which are of the form

$$u(r, \phi, z > 0) \propto \exp(\mathrm{i}k_z z) \exp(\mathrm{i}m\phi) \cdot J_m(k_r r). \quad (3)$$

Soon after the discovery of Bessel beams as formal solutions to a differential equation the following intuitive explanation was found for the diffraction-free property of Bessel beams [2]. This explanation also provides an elegant interpretation of the function $A(\phi)$.

Any light beam can be described as a superposition of plane waves of the form $\exp(\mathrm{i}(k_x x + k_y y + k_z z))$. On propagation over a distance Δz each plane-wave component suffers an individual phase shift of $k_z \Delta z$. In general, different plane-wave components suffer different phase shifts, so their interference pattern, i.e. the light beam, changes shape. (This mechanism is the basis of frequently used beam propagation algorithms; see for example [9].) However, there are special cases in which the plane-wave components always stay in phase, namely when the phase shift $k_z \Delta z$ is the same for every plane-wave component. Such light beams do not change on propagation, not even in scale. (Note that structurally stable beams such

[4] Present address: Instituto Nacional de Astrofisica, Optica y Electrónica, Apartado Postal 51/216, Puebla, Mexico 72000.

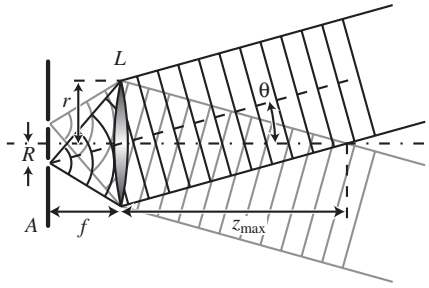

Figure 1. Generation of diffraction-free beams through illumination of a centred thin ring in the front focal plane of a lens. The lens converts the light from each bright point on the ring into a plane wave, whereby all the plane waves from points on the ring travel at the same angle θ with respect to the optical axis. Any superposition of plane waves with the same propagation angle θ is diffraction-free in the cone-shaped region of length z_{max} behind the lens in which they intersect.

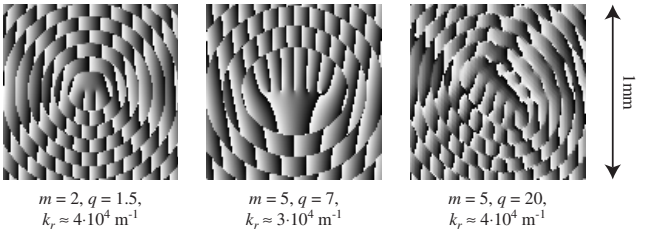

Figure 2. Greyscale representation of the optical thickness of some Mathieu-beam holograms. Ideally, the range of grey levels corresponds to phase delays ranging all the way from 0 to 2π. In the hologram corresponding to $m = 5, q = 20$ the innermost vortices lie along a straight line inclined by 45° with respect to the direction of the blaze (horizontal), while in the remaining holograms the vortices are arranged along the x axis. In all cases, the horizontal wavenumber is $k_x \approx 6 \times 10^4$, which, for a wavelength of $\lambda = 633$ nm, corresponds to a first-order diffraction angle of approximately 0.3°.

as, for example, the Hermite–Gaussian or Laguerre–Gaussian modes, *do* change in scale.) This condition is satisfied for monochromatic light if all the components have the same k_z, which in turn means that all the components are inclined with respect to the optical axis by the same angle, θ. The variable k_z in equation (1) is precisely the k_z of all the individual plane-wave components in such a beam, while the variable k_r, which is given by

$$k_r = \sqrt{k_x^2 + k_y^2} \tag{4}$$

is therefore simply the transverse wave number of all the plane-wave components. Such a light beam can easily be generated by illuminating with monochromatic light a thin annular aperture centred in the front focal plane of a lens (figure 1). The function $A(\phi)$ simply describes the field distribution on this thin annulus.

Recently closed-form expressions for $u(x, y)$ [10] and $A(\phi)$ [11] were found for an interesting family of diffraction-free light beams, the so-called Mathieu beams, which are the elliptical generalizations of Bessel beams. Just as Bessel beams are related to the TE and TM modes of circular waveguides, so Mathieu beams are related to the TE and TM modes of elliptical waveguides [12]. These are, in turn, the optical analogues of many dynamical systems with elliptical symmetry, such as elliptical membranes [13].

Mathieu beams are characterized by the 'ellipticity' parameter q, and the integer m, which is termed the mode order or charge. Bessel beams, which are circularly symmetric, represent the limiting case when $q = 0$, and the centre of the beam then contains a so-called optical vortex of charge m. A vortex is a screw dislocation in the phase front of the beam, the pitch of which is m wavelengths, which corresponds to a phase change of $2\pi m$ around the vortex centre [14, 15]. For a moderate increase in q, the mth-order vortex separates into m vortices of order 1, all of which are positioned close to the beam axis. As q increases beyond a critical value given by $q_c \approx m^2/2 - 1$ [11], numerous additional vortices appear in various positions across the beam.

Approximations to zero-order ($m = 0$) Mathieu beams have previously been created experimentally by illuminating a thin annular aperture in the back focal plane of a lens with an elongated Gaussian beam [16]. In this paper we report the first experimental generation of higher-order Mathieu beams. We also investigate the effect of one particular property associated with the vortices in Mathieu beams, namely their orbital-angular-momentum (OAM) content. We discuss a number of methods to calculate the OAM per photon in diffraction-free beams and present the numerically calculated OAM content of all Mathieu beams within a large area of parameter space.

2. Holographic generation of Mathieu beams

The first holographic generation of Bessel beams was reported in [8, 17]. It was confirmed that the beams produced in this way had the anticipated properties, in particular propagation invariance.

In this paper, we use computer-generated phase holograms designed to represent the phase distribution of the desired Mathieu beam, propagating at a small angle to the optical axis (figure 2). These holograms are manufactured by first creating a photographic negative of a greyscale representation of this phase distribution (using a slide writer), making a contact print onto holographic film, which is then 'bleached', thereby transforming the grey level into optical thickness (the exact process used in this work is described in [18]; a similar 'recipe' for bleaching can be found in [19]). If the range of optical thicknesses in the finished hologram correspond to phase delays covering a range of width 2π, a plane wave of uniform intensity passing through the hologram would simply have the phase structure of an inclined Mathieu beam and travel in the direction of the inclination. However, in practice the hologram introduces phase delays over a significantly different range. As a result, the beam splits into diffraction orders behind the hologram (figure 3), just like a beam behind a grating. The first diffraction order is the desired inclined beam, which is picked out from the beam with a circular aperture, A_2, in the back focal plane of a lens, L_1, which is positioned such that the hologram, H, is in its front focal plane (figure 3). This first-order diffracted beam is then passed through a second lens, L_2, which, together with L_1, forms a beam telescope. At the same time the lenses are arranged such that the plane of the hologram is imaged into the second lens's back focal plane, H′.

Note that in the back focal plane of lens L_1 (figure 4), the intensity distribution of the first-order beam is an almost

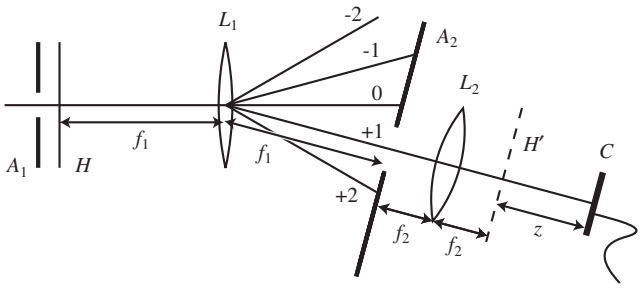

Figure 3. Schematic of the experiment for the holographic generation of higher-order Mathieu beams. The phase hologram H is illuminated by a beam truncated by the circular aperture A_1. In the focal plane of lens L_1 the circular aperture A_2 picks out the bright ring of the first diffraction order, which is then turned into a diffraction-free beam by the lens L_2. The CCD array C allows the intensity cross sections of the resulting beam to be recorded at various distances z behind the image of the hologram, H′. The focal lengths used in our experiment were $f_1 = 600$ mm and $f_2 = 250$ mm.

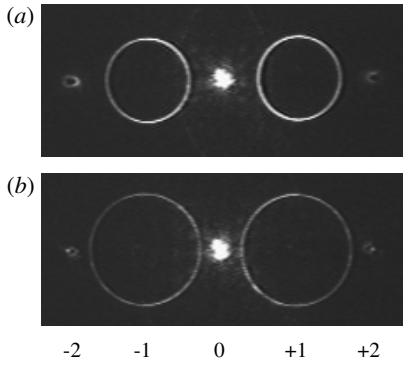

Figure 4. Experimentally recorded intensity cross sections in the focal plane of a lens behind Mathieu-beam phase holograms under top-hat illumination for $k_r = 3 \times 10^4$ m^{-1} (recorded behind $m = 5$ and $q = 7$ hologram, see figure 2) (*a*) and for $k_r = 4 \times 10^4$ m^{-1} (recorded behind $m = 5$ and $q = 20$ hologram) (*b*). The diffraction orders are identified at the bottom.

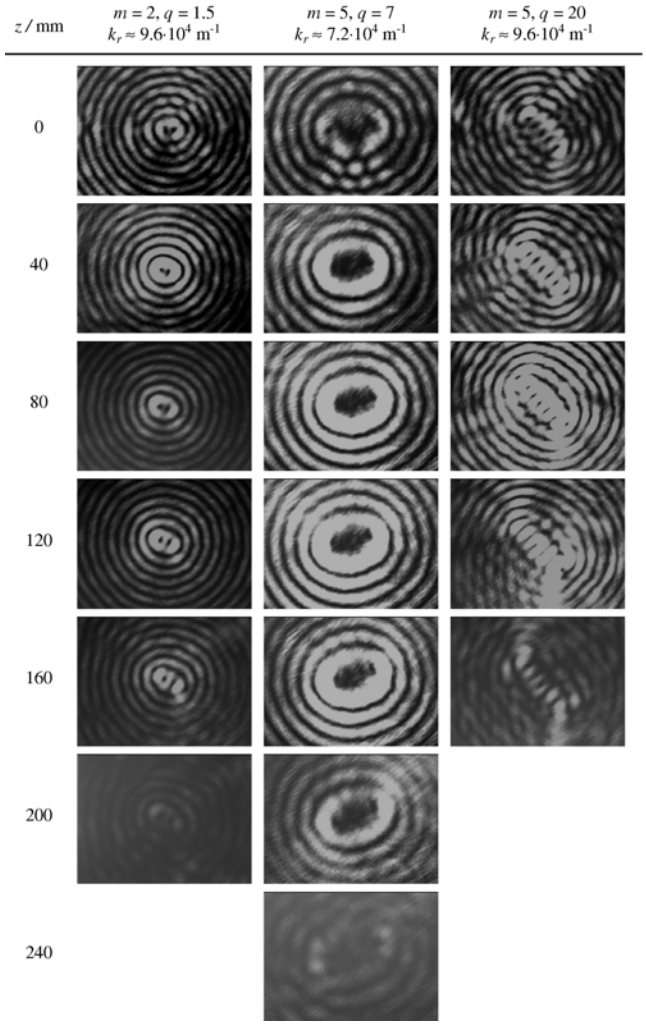

Figure 5. Intensity cross sections of different experimentally generated higher-order Mathieu beams at different distances z behind the plane H′ (see figure 3). The three different beams correspond to the three holograms shown in figure 2. The area represented by each image is approximately 0.5 mm by 0.4 mm.

perfect circle. As this plane also happens to be the front focal plane of lens L_2, our set-up is essentially of the type shown in figure 1; the first part of the set-up, including illumination, hologram, lens L_1, and aperture A_2, is therefore simply a way of creating, in the front focal plane of lens L_2, a ring-shaped light field with the azimuthal field dependence $A(\phi)$ that leads to a Mathieu beam behind the lens.

Figure 5 shows intensity cross sections through the Mathieu beams produced with the holograms shown in figure 2. It can clearly be seen that the beams are diffraction free only over a finite distance, z_{max}, the so-called propagation-invariant region, behind which the centre of the beam rapidly becomes fainter. This is a well known effect due to the finite size of the beam. The slight rotation about the optical axis within the propagation-invariant region, which can also be seen in figure 5, has been predicted theoretically very recently [11] and is also due to the beam's finite size. The distance $z_{\max}$ can be estimated geometrically to be the length of the cone in which all the plane-wave components in the beam intersect (see figure 1), which is given by [1]

$$z_{max} = \frac{r}{\tan\theta}. \tag{5}$$

Here r is the radius of the beam in the plane of the aperture (the base of the cone) and θ is the inclination angle of the beam's plane-wave components with respect to the optical axis. The relevant aperture in our experiment is the image of A_1 in the plane H′, which has a radius of $r \approx 1.6$ mm (the radius of A_1 is about 3.75 mm, and its image in the plane H′ is magnified by a factor of $M = -f_2/f_1 \approx -0.42$). The angle θ can be calculated from the equation $\tan\theta \approx \sin\theta = k_r/k$, which in our experiment evaluated to $\theta \approx 0.55°$ and $\theta \approx 0.42°$ for holograms with $k_r = 4 \times 10^4$ m^{-1} and $k_r = 3 \times 10^4$ m^{-1}, respectively. (Note that imaging the beam from the plane H into the plane H′ with magnification M changes k_r by a factor $1/|M|$.) These values lead to respective diffraction-free distances of $r_{max} \approx 162$ mm (for $\theta \approx 0.55°$) and $r_{max} \approx 215$ mm ($\theta \approx 0.42°$), which are in good agreement with the distances after which the centre of the beams in our experiment became much fainter (figure 5).

Figure 6 shows interference patterns between the Mathieu beams and an inclined plane wave, illustrating the phase structure of the beams. The plane wave was obtained by also allowing the zeroth-order diffracted beam to pass through the aperture A_2. Comparison with figure 2 confirms that the beams

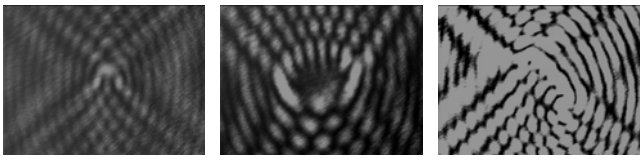

$m = 2$, $q = 1.5$ $k_r \approx 9.6{\cdot}10^4$ m^{-1} | $m = 5$, $q = 7$ $k_r \approx 7.2{\cdot}10^4$ m^{-1} | $m = 5$, $q = 20$ $k_r \approx 9.6{\cdot}10^4$ m^{-1}

Figure 6. Interference of higher-order Mathieu beams with a plane wave. All the images were taken a distance $z = 80$ mm behind the plane of the hologram. The area represented by each image is approximately 0.5 mm by 0.4 mm.

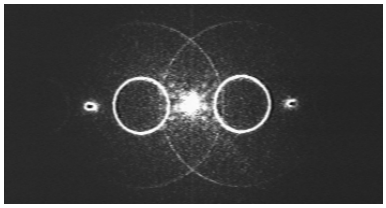

Figure 7. Over-exposed version of figure 4(*a*), showing 'harmonic rings' around the first-order rings.

do indeed have the phase structure of higher-order Mathieu beams.

It is perhaps worth mentioning an important complication that often occurs in holographic beam-generation set-ups that use a phase hologram to impart the right phase structure onto the transmitted beam: usually the intensity cross section of the beam illuminating the hologram is different from that of the desired beam. In our experiment, for example, we seek to generate beams whose intensity distribution is that of bright, centred, distorted rings, and yet we illuminate the hologram with a top-hat intensity profile. Like the erroneous phase-step height, this 'wrong' intensity profile gives rise to distinct features in the far-field diffraction pattern (or in the focal plane of a lens); the former leads to a non-zero intensity in diffraction orders other than the desired +1st order, the latter, at least in the case of our experiment, gives rise to additional 'harmonic' rings around the first-order 'fundamental' rings with a radius that is about three times larger (figure 7).

These harmonic rings can be understood as corresponding to sharp peaks in the Hankel transform of the radial amplitude distribution behind the hologram,

$$A_m(k_r) = \int_0^\infty A(r) J_m(k_r r) r \, \mathrm{d}r \tag{6}$$

which is essentially a decomposition of the beam in terms of mth-order Bessel beams with different values of k_r. Some intuitive insight into the origin of these rings, formulated in terms of the somewhat more familiar Fourier transform, can be gained by considering the following qualitative argument, which also explains the adjective 'harmonic'. The radial intensity dependence of Mathieu beams is that of a more-or-less regular oscillation, more specifically the kind of oscillation whose far-field diffraction pattern (i.e. Fourier transform) is a thin bright ring. If one accepts that the relationship between the radial profile of the beam (oscillations) and that of its Fourier transform (a sharp peak) is analogous to the relationship between a perfect, one-dimensional sine oscillation and its Fourier transform (a 'δ' peak) it will not be difficult to believe

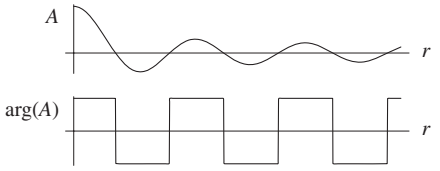

Figure 8. Radial amplitude distribution and corresponding phase of a zeroth-order Bessel beam, a particularly simple example of a Mathieu beam. A phase hologram of such a beam turns uniform plane-wave illumination into a beam with a radial amplitude dependence in the form of a square wave.

that the Fourier transform of the beam behind a Mathieu-beam hologram under uniform plane-wave illumination, which has a square-wave-type radial amplitude dependence (figure 8) has a radial profile with features similar to those of the Fourier transform of a one-dimensional square wave. The phase distribution makes the radial amplitude distribution periodic; this is the reason for the occurrence of relatively narrow harmonic rings. Note that there is no 'harmonic ring' with twice the radius of the 'fundamental ring'; this is mirrored by the fact that the Fourier coefficients of a square wave corresponding to even multiples of the fundamental frequency are all zero. Also note that the 'wrong' illumination of any phase hologram generally leads to additional features in the far-field diffraction pattern; the case of diffraction-free beams is an interesting example because these additional features take on a particularly simple form.

3. Calculation of the OAM per photon of diffraction-free beams

In the introduction the OAM associated with the vortices in Mathieu beams was highlighted. In this section numerical methods are developed that allow the calculation of the OAM of Mathieu beams in section 4.

The component of a light beam's OAM in the direction of propagation is related to the polarization-independent transverse components of its (vector) momentum density. According to equation (9) in [20], which was derived using the paraxial approximation, these components of the momentum density are

$$\vec{p}_L = \mathrm{i}\omega \frac{\epsilon_0}{2}((u^*)\vec{\nabla}u - u(\vec{\nabla}u^*)) = -\omega\epsilon_0 \mathrm{i}m((u^*)\vec{\nabla}u) \tag{7}$$

where $u(x, y)$ is an amplitude cross section through the beam. The corresponding flux of the OAM[5] is

$$l_z = |\vec{r} \times \vec{p}_L|. \tag{8}$$

It is convenient to introduce the *local OAM per photon*, δl_z, defined by equating its ratio to the photon energy with the ratio of l_z to the energy density $w(x, y) = |u(x, y)|^2$. Note that the term is based on a semiclassical interpretation of the quantities involved. The OAM per photon in the beam, δL_z, can be written as the integral over the local OAM per photon, δl_z, weighted by the normalized energy density (or intensity), namely

$$\delta L_z = \frac{\iint \delta l_z(x, y)|u(x, y)|^2 \, \mathrm{d}x \, \mathrm{d}y}{\iint |u(x, y)|^2 \, \mathrm{d}x \, \mathrm{d}y}. \tag{9}$$

[5] In the following all angular momenta are understood to be the component in the propagation direction.

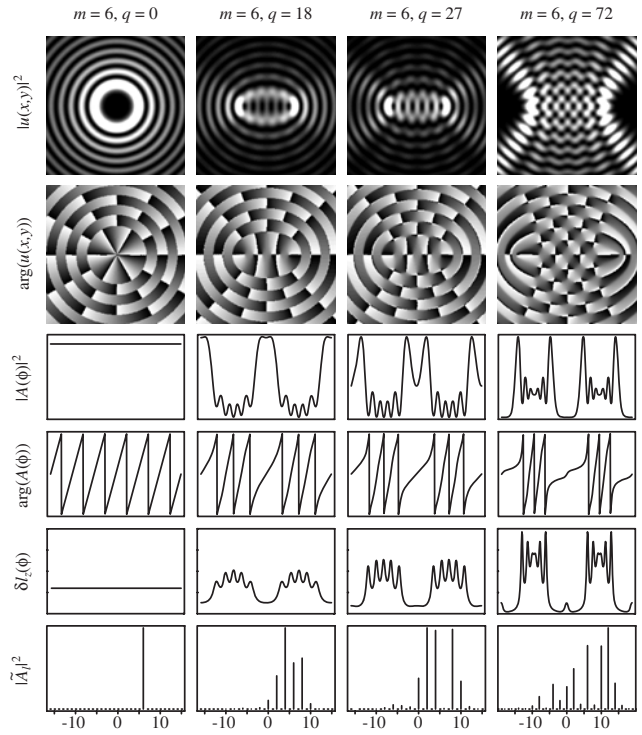

Figure 9. Examples of Mathieu beams and calculation of their orbital angular momenta. In the back focal plane of a lens, the Mathieu beams described by the functions $u(x, y)$ (shown are the intensity and phase cross sections, $|u(x, y)|^2$ and $\arg(u(x, y))$) are thin bright rings with an angular amplitude distribution of the form $A(\phi)$ (again, the intensity and phase distributions are shown over the full ϕ range between 0 and 2π). The local OAM per photon, $\delta l_z(\phi)$ (the vertical range corresponds to values between 0 and $20\hbar$), can be calculated from $\arg(A(\phi))$. The power spectra of $A(\phi)$, $|\tilde{A}_l|^2$, are also the Bessel-beam spectra of the corresponding Mathieu beams. The respective orbital angular momenta per photon, δL_z, are $6\hbar$ ($q = 0$), $4.92\hbar$ ($q = 18$), $4.40\hbar$ ($q = 27$) and $6.32\hbar$ ($q = 72$). In the case $q = 72$ numerous additional vortices can be spotted in the beam's phase cross section, $\arg(u(x, y))$.

Note that regions of zero intensity, such as for example the cylindrical surfaces of zero-field amplitude in Bessel beams, do not contribute to δL_z—the density of OAM is zero there.

When calculating the OAM content of perfectly diffraction-free light beams, it is useful to be aware of some of their peculiarities. Most importantly, perfectly diffraction-free light beams are infinitely wide—this is the reason why experimental realizations of diffraction-free beams, which are always limited by a finite aperture, can only ever be approximations and do exhibit diffraction effects, such as the finite range of 'diffraction-free' propagation observed in section 2 [2]. Closely related to their infinite width is the infinite energy content of perfectly diffraction-free light beams. Bessel beams, for example, have approximately the same—finite—amount of energy in each of the concentric bright rings, of which there are infinitely many [1]. As the OAM per photon, δL_z, is proportional to the ratio of OAM and energy, perfectly diffraction-free beams with non-zero values of δL_z therefore possess an infinite OAM.

Perhaps the following subtle point merits a brief discussion: the OAM flux (equation (8)) was calculated with respect to the origin. At first this might appear to restrict

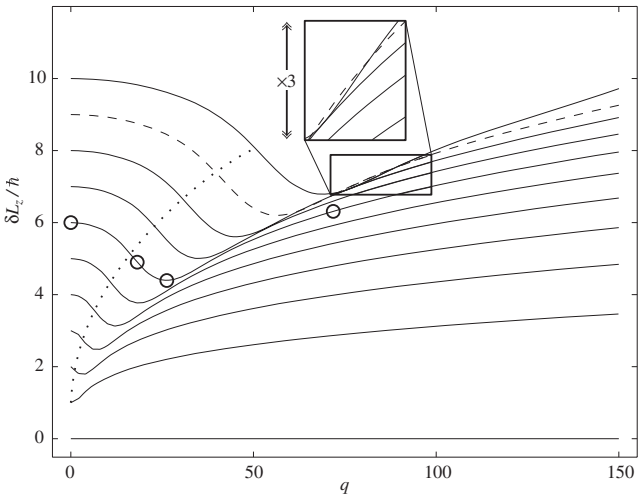

Figure 10. OAM per photon, δL_z, of Mathieu beams with m indices between 0 and 10, plotted as a function of q. The curve corresponding to a specific value of m starts off at $q = 0$ with a value $\delta L_z(0) = m\hbar$. The dotted line crosses these curves approximately at the critical values q_c. The circles mark the cases that are shown in more detail in figure 9.

the generality of this approach; however, as the OAM of a light beam in the direction of the beam's propagation direction (more precisely the direction of the momentum vector of the entire beam) is independent of the choice of axis and therefore intrinsic [21], it does not matter relative to which axis it is calculated, as long as the axis is parallel to the beam's propagation direction.

Numerically, the gradients in equation (7) can be approximated by finite differences, for example in the form $\partial u/\partial x \approx (u(x + \Delta, y) - u(x - \Delta, y))/(2\Delta)$, and the integration in equation (9) can be replaced by a summation over a discrete number of values. The OAM per photon can therefore be calculated quite easily from values of $u(x, y)$ at a finite number of points on a beam cross section.

It can be shown that in polar coordinates the expression for δl_z becomes

$$\delta l_z(r, \phi) = \frac{\mathrm{d}\Phi(r, \phi)}{\mathrm{d}\phi} \cdot \hbar \tag{10}$$

where $\Phi(r, \phi)$ is the phase cross section of the light beam. (For the local OAM per photon of a light beam with an azimuthal phase dependence of the form $\Phi(\phi) = l\phi$ this gives $\delta l_z = l\hbar$ everywhere and therefore $\delta L_z = l\hbar$, as expected [20]. As their azimuthal phase term is of the form $\exp(\mathrm{i}m\phi)$, Mathieu beams with $q = 0$ (i.e. Bessel beams) have an azimuthal phase dependence of the form $\Phi(\phi) = m\phi$ and therefore an OAM per photon of $\delta L_z = m\hbar$.) For diffraction-free beams, this expression can be evaluated in the far field, where the intensity cross section is simply a bright circle. In terms of the field distribution on this circle, $A(\phi)$, equation (10) becomes

$$\delta l_z(\phi) = \frac{\mathrm{d}}{\mathrm{d}\phi} \arg(A(\phi)) \cdot \hbar. \tag{11}$$

Figure 9 shows some examples of intensity and phase cross sections through Mathieu beams, alongside the corresponding functions $A(\phi)$ and the local OAM per photon, $\delta l_z(\phi)$.

Note that care has to be taken with 2π phase jumps in the function $\arg(A(\phi))$.

A completely different approach for the calculation of the OAM per photon in a light beam involves a decomposition in terms of beams components with known orbital angular momenta, like for example Laguerre–Gaussian beams or Bessel beams (equation (3)), which have an azimuthal phase term of the form $\exp(\mathrm{i}l\phi)$, i.e. an azimuthal phase dependence $\Phi(\phi) = l\phi$, and therefore an OAM per photon of $l\hbar$. The sum of the per-photon orbital angular momenta of these individual beam components, weighted by the corresponding relative intensities, is the OAM per photon of the beam as a whole.

Diffraction-free beams are special in that they can be decomposed very easily in terms of Bessel beams: a Fourier transform of the azimuthal amplitude distribution in the far field (or at the focus of a lens), $A(\phi)$, taking into account that $A(\phi)$ is 2π-periodic, yields the discrete set of Fourier coefficients $\tilde{A}_l$ of the $\exp(\mathrm{i}l\phi)$ components of the beam (equation (47) in [22]). The OAM per photon in the beam is simply

$$\delta L_z = \frac{\sum_l l|\tilde{A}_l|^2}{\sum_l |\tilde{A}_l|^2} \cdot \hbar. \tag{12}$$

Alongside beam cross sections, $u(x, y)$, azimuthal field distributions in the far field, $A(\phi)$, and corresponding local orbital angular momenta per photon, figure 9 also shows a representation of the Fourier coefficients, $\tilde{A}_l$, for some Mathieu beams.

4. Orbital angular momentum of Mathieu beams

In light beams with a phase structure of the form $\exp(\mathrm{i}l\phi)$, like for example Bessel beams, the local OAM per photon, δl_z, has the constant value $l\hbar$ everywhere, which is also the value of the beam's OAM per photon, δL_z. This is not the case in Mathieu beams, which exhibit a much more complex phase structure.

Figure 10 shows plots of δL_z as a function of q for Mathieu beams with $m = 0, 1, \ldots, 10$; for negative values of m, δL_z simply changes sign. The curves were obtained by calculating the m coordinate of the centre of gravity of the power spectrum of $A(\phi)$, as outlined in section 3. Apart from the curve for $m = 0$, which is zero everywhere, the curves all start from $\delta L_z = m\hbar$ at $q = 0$ and, as q increases, smoothly decrease, pass through a minimum, and increase again, sometimes crossing the curve for a different value of m. For $m = \pm 1$, the minimum appears to be located at $q = 0$. The curves are continuous everywhere, including at the critical values q_c, where numerous new vortices start to appear in the beam.

5. Conclusions

We have reported the first experimental generation of higher-order Mathieu beams. We show that important properties of the holographic method used are illustrated very clearly when applied to diffraction-free beams; in particular, the effect of uniform illumination of the hologram manifests itself in the far field in the form of 'radial harmonics', i.e. additional rings whose radius is an integer multiple of the 'fundamental' ring. We have also calculated the OAM content of all Mathieu beams within a large area of parameter space.

Acknowledgments

SC-C acknowledges support by the Engineering and Physical Sciences Research Council (grant no GR/N37117/01). This work was partially supported by Consejo Nacional de Ciencia y Tecnologia. MJP and JC acknowledge support from the Royal Society.

References

[1] Durnin J 1987 Exact solutions for nondiffracting beams: I. The scalar theory *J. Opt. Soc. Am.* A **4** 651–4
[2] Durnin J, Miceli J J J and Eberly J H 1987 Diffraction-free beams *Phys. Rev. Lett.* **58** 1499–501
[3] Erdélyi M, Horváth Z L, Szabó G, Bor S, Tittel F K, Cavallaro J R and Smayling M C 1997 Generation of diffraction-free beams for applications in optical microlithography *J. Vac. Sci. Technol.* B **15** 287
[4] Lu J-Y and He S 1999 Optical X wave communications *Opt. Commun.* **161** 187–92
[5] Lu J-Y and Greenleaf J F 1994 A study of two-dimensional array transducers for limited diffraction beams *IEEE Trans. Ultrason. Ferroelectr. Freq. Control* **41** 724–39
[6] Whittaker E T 1902 On the partial differential equations of mathematical physics *Math. Ann.* **57** 333–55
[7] Whittaker E T and Watson G N 1927 *A Course of Modern Analysis* 4th edn (Cambridge: Cambridge University Press) ch XVIII–XIX
[8] Vasara A, Turunen J and Friberg A T 1989 Realization of general nondiffracting beams with computer-generated holograms *J. Opt. Soc. Am.* A **6** 1748–54
[9] Sziklas E A and Siegman A E 1975 Mode calculation in unstable resonators with flowing saturable gain: 2: Fast Fourier transform method *Appl. Opt.* **14** 1874–89
[10] Gutiérrez-Vega J C, Iturbe-Castillo M D and Chávez-Cerda S 2000 Alternative formulation for invariant optical fields: Mathieu beams *Opt. Lett.* **25** 1493–5
[11] Chávez-Cerda S, Gutiérrez-Vega J C and New G H C 2001 Elliptic vortices of electromagnetic wavefields *Opt. Lett.* **26** 1803–5
[12] Gutiérrez-Vega J C, Rodríguez-Dagnino R and Chávez-Cerda S 2002 Attentuation characteristics in confocal annular elliptic waveguides and resonators *IEEE Trans. Microwave Theory and Techniques* at press
[13] McLachlan N W 1951 *Theory and Applications of Mathieu Functions* (London: Clarendon)
[14] Berry M 1981 Singularities in waves and rays *Les Houches Lecture Series Session XXXV* ed R Balian, M Kléman and J-P Poirier (Amsterdam: North-Holland) pp 453–543
[15] Soskin M S and Vasnetsov M V 2001 Singular optics *Prog. Opt.* **42** 219–76
[16] Gutiérrez-Vega J C, Iturbe-Castillo M D, Tepichín E, Rodríguez-Dagnino R M, Chávez-Cerda S and New G H C 2001 Experimental demonstration of optical Mathieu beams *Opt. Commun.* **195** 35–40
[17] Turunen J, Vasara A and Friberg A T 1988 Holographic generation of diffraction-free beams *Appl. Opt.* **27** 3959–62
[18] O'Neil A T 2001 *PhD Thesis* University of St Andrews
[19] Bjelkhagen H I 1993 *Silver-Halide Recording Materials* (Berlin: Springer) ch 5
[20] Allen L, Beijersbergen M W, Spreeuw R J C and Woerdman J P 1992 Orbital angular momentum of light and the transformation of Laguerre–Gaussian modes *Phys. Rev.* A **45** 8185–9
[21] Berry M 1998 Paraxial beams of spinning light *Singular Optics* ed M S Soskin *Proc. SPIE* **3487** (SPIE Int. Soc. Opt. Engng.) (Bellingham, Washington, USA) pp 1–5
[22] Siegman A E 1986 *Lasers* (Mill Valley, CA: University Science Books)